Special Double Issue Article

Nicholas A. Mecholsky, Bothina Hamad*, Lorenzo Resca, Ian L. Pegg and Marco Fornari

Anisotropy Effects on the Thermoelectric Electronic Transport Coefficients

Abstract: Engineering thermoelectric (TE) materials for applications in power generation and cooling requires an understanding of how anisotropy influences the TE properties. In this paper we use an angular-dependent, multivalley formalism to model the band structure and to explore the effect of anisotropy on the Seebeck and conductivity tensors. Specifically we explore the effect of degeneracy and relative orientation of the effective mass ellipsoids near critical points on the shape of these tensors. Examples of these types of anisotropic effects are explored within the above formalism and with the full band structures of two materials: half-Heusler ZrNiSn and (Sr,Ba) Nb_2O_6 with the tetragonal tungsten bronze structure.

Keywords: Thermoelectric materials, Anisotropy, Boltzman transport theory

DOI 10.1515/ehs-2014-0041

Introduction

The discovery of high-performance thermoelectric (TE) materials and the technological transfer to energy recovery systems and solid-state refrigerators is complicated by several requirements that must be simultaneously satisfied by both the p-type and n-type legs of the thermocouples. First of all, the p-type and n-type materials must exhibit compatible thermo-mechanical properties with the metal electrodes and between themselves. Then, the figure of merit ($ZT = \frac{\sigma S^2}{\kappa} T$, where κ is the thermal conductivity, S the Seebeck coefficient, and σ the electrical conductivity) of each material component must be maximized at the proper operating temperature, T, in order to reach sufficient efficiency in the conversion process.

The guiding principles to optimize the bulk material properties usually involve lowering the lattice thermal conductivity using dynamic and/or static disorder (mostly cage filling and alloying) and improving the charge transport by tuning the band structure. This last task is rationalized using the isotropic free-electron model (Ashcroft and Mermin 1976; Grosso and Pastori Parravicini 2000; Singleton 2001) usually in a single-band (valley) configuration. Within these assumptions ($\sigma \sim \frac{\rho}{m^*}$ and $S \sim \frac{m^*}{\rho^{2/3}}$, m^* being the effective mass and ρ the carrier density), a delicate balance should be reached between σ and S to optimize the numerator of the figure of merit (Nolas, Sharp, and Goldsmid 2001; Kanatzidis 2009; Nolas, Poon, and Kanatzidis 2006). Indeed, large effective masses favor the enhancement of the Seebeck coefficients but limits the electrical conductivity. The electronic component of the thermal conductivity, because of the Wiedemann–Franz law, $\frac{\kappa_e}{\sigma} \sim L_0 T$ (where L_0 is the Lorentz number) is controlled by σ.

The key concept, used in applying the free-electron model, is the effective mass approximation. The effective mass represents the band structure in proximity to a local extremum in the Brillouin zone (BZ) and corresponds to the quadratic term of the Taylor expansion of the energy dispersion for a band n, $E_n(\mathbf{k})$, near such a local extremum, $\mathbf{k}_0$. By its very nature the inverse effective mass, $\mathbb{M}^{-1}$, is a second-rank tensor defined from the second partial derivatives computed in $\mathbf{k}_0$:

$$\mathbb{M}^{-1}_{i,j} = \frac{m_e}{\hbar^2} \frac{\partial^2 E_n(\mathbf{k})}{\partial k_i \partial k_j}\bigg|_{\mathbf{k}_0}. \quad [1]$$

Its tensorial character, however, is often neglected although it leads to interesting concepts to understand and optimize bulk TE materials.

In this manuscript, we will discuss the main consequences associated with the tensorial nature of the effective mass (in Section “Electronic Transport Tensors”) as well as the interplay between the multivalley nature of the band structure and the TE transport tensors (in Section “Effect of Multivalley Band Structure”). We

*Corresponding author: **Bothina Hamad,** Department of Physics, University of Jordan, Queen Rania St, Amman 11942, Jordan; Department of Physics, University of Arkansas, 825 W. Dickson St., Fayetteville, AR 72701, USA, E-mail: bothinah@uark.edu
Nicholas A. Mecholsky, Lorenzo Resca, Ian L. Pegg, Department of Physics and Vitreous State Laboratory, The Catholic University of America, Washington, DC, USA
Marco Fornari, Department of Physics, Central Michigan University, Mount Pleasant, MI, USA

focus on the consequences associated with the features of the band structure without discussing the well-established role of crystal symmetry on the tensors. The intuition provided by analytical models is compared with selected first principle calculations in Section "Considerations on Realistic Band Structures".

Electronic Transport Tensors

In the Boltzmann transport theory within the scattering relaxation-time approximation, the electronic transport coefficients[1] can be written as

$$\underline{\boldsymbol{\sigma}} = \underline{\mathscr{L}}^{(0)}, \tag{2a}$$

$$\underline{\boldsymbol{S}} = \frac{-1}{Te}\left(\underline{\mathscr{L}}^{(0)}\right)^{-1}.\underline{\mathscr{L}}^{(1)}, \tag{2b}$$

$$\underline{\boldsymbol{\kappa}} = \frac{1}{Te^2}\left(\underline{\mathscr{L}}^{(2)} - \underline{\mathscr{L}}^{(1)} \cdot \left(\underline{\mathscr{L}}^{(0)}\right)^{-1} \cdot \underline{\mathscr{L}}^{(1)}\right), \tag{2c}$$

where T is the temperature and e is the absolute value of the electron charge. Those tensors in turn contribute to TE figures of merit, the most common of which is ZT, tensorially expressed as $\underline{\boldsymbol{S}}^T \cdot \underline{\boldsymbol{\sigma}} \cdot \underline{\boldsymbol{S}} \cdot \underline{\boldsymbol{\kappa}}^{-1} T$.

Following Mecholsky et al. (2014) we adopt an angular effective mass approach and write the transport tensors above in terms of

$$\left[\underline{\mathscr{L}}_c^{(\alpha)}\right]_{i,j} = \frac{e^2\sqrt{m_e}}{2^{3/2}\pi^3\hbar^3}\int_{E_c}^{\infty}(E-\mu)^{\alpha}\left(-\frac{\partial f_0}{\partial E}\right)(E-E_c)^{3/2}C_{c\,i,j}\,dE \tag{3}$$

for a conduction-like band and

$$\left[\underline{\mathscr{L}}_v^{(\alpha)}\right]_{i,j} = \frac{e^2\sqrt{m_e}}{2^{3/2}\pi^3\hbar^3}\int_{-\infty}^{E_v}(E-\mu)^{\alpha}\left(-\frac{\partial f_0}{\partial E}\right)(E_v-E)^{3/2}C_{v\,i,j}\,dE \tag{4}$$

for a valence-like band (f_0 being the Fermi–Dirac distribution function).

In eqs [3] and [4] we have introduced, for each band n, a constant tensor with matrix elements

$$[\underline{\mathbf{C}}_n]_{i,j} = C_{n\,i,j} = \sum_q \int_0^{2\pi}\int_0^{\pi} \frac{\hat{v}_{n,i}(\theta,\phi)[\underline{\boldsymbol{\tau}}_n]_{j,q}\hat{v}_{n,q}(\theta,\phi)}{2|f_n(\theta,\phi)|^{5/2}}\sin\theta\,d\theta\,d\phi, \tag{5}$$

which will prove to be essential for the development of our analysis. Its definition in eq. [5] involves a particularly weighted average over the angular effective mass function $f_n(\theta,\phi)$ defined for a band n in the proximity of a band extremum as

$$E_n(k_r,\theta,\phi) \simeq E_{n0} + \frac{\hbar^2 k_r^2}{2m_e} f_n(\theta,\phi). \tag{6}$$

The weighted average in eq. [5] over that angular function captures the essential effects of the electronic structure, including band warping, on all related transport coefficients. $\underline{C}_n$ must be a symmetric tensor (Mecholsky et al. 2014). We thus have six independent integrals for each band contributing to the electronic transport. A band will contribute to transport if the band extremum is within a few k_BT of the chemical potential.

Assuming, as it is conventional, a constant relaxation time, the Boltzmann transport expression for a simple two-band model can be written as

$$\begin{aligned}\left[\underline{\mathscr{L}}^{(\alpha)}\right]_{i,j} &= \tau_c \mathscr{C}_{c\,i,j} K_\alpha(\beta(E_c-\mu),\beta) \\ &\quad + (-1)^{\alpha}\tau_v \mathscr{C}_{v\,i,j} K_\alpha(\beta(\mu-E_v),\beta),\end{aligned} \tag{7}$$

where we define "universal" functions K_α as

$$K_\alpha(s,\beta) = \frac{e^2\sqrt{m_e}}{2^{3/2}\pi^3\hbar^3\beta^{\alpha+3/2}}\int_s^{\infty}\frac{x^{\alpha}(x-s)^{3/2}e^x}{(1+e^x)^2}\,dx, \tag{8}$$

and $\underline{\mathscr{C}}$ is $\underline{C}$ of eq. [5] with the explicit relaxation-time dependence factored out. The integrals in K_α may also be expressed in terms of standard Fermi–Dirac integrals.[2] The generalization to a multiband cases is

$$\left[\underline{\mathscr{L}}^{(\alpha)}\right]_{i,j} = \sum_{n=1}^{N_b}(\chi_n)^{\alpha}\tau_n K_\alpha(\chi_n\beta(E_n-\mu),\beta)\mathscr{C}_{n\,i,j}. \tag{9}$$

Within this approach we model the band structure as a set of N_b conduction-(valence-) like ellipsoidal bands with minima (maxima) at energy E_n. The positive or negative curvature is determined by $\chi_n = \pm 1$. Within the general theory above, in the case of an ellipsoidal band, the $\underline{\mathscr{C}}$ tensor calculation gives

$$\left[\underline{\mathscr{C}}_{\text{ellipsoid}}\right]_{i,j} = \left(\frac{8\pi}{3}\frac{\sqrt{m_1 m_2 m_3}}{m_i\sqrt{m_e}}\right)\delta_{i,j}, \tag{10}$$

where $m_{1,2,3}$ denote the effective masses in the x, y, z principal directions, $\delta_{i,j}$ is the Kronecker symbol and no summation convention is implied over the repeated i index.

We may use this as a starting point in our discussion of anisotropy. Plugging a single ellipsoidal $\underline{\mathscr{C}}$ into eq. [9],

1 The last expression for the electron thermal conductivity is included for completeness.

2 Consideration of at least energy-dependent isotropic relaxation times $\tau_n(E)$ would clearly alter the basic definition of eq. [8], but only in a manner that would not substantially modify our following results and discussions (see Mecholsky et al. 2014).

we can derive expressions for the transport equations using eq. [2]. It is instructive to compare the asymptotic expansions for the eigenvalues of the conductivity and the thermopower tensors when, on the scale of k_BT, the chemical potential μ lies sufficiently outside either conduction and valence bands (insulator limit) or when the chemical potential lies within a given band (metallic limit). In the insulator limit

$$[\underline{\boldsymbol{\sigma}}]_{i,j} \sim \frac{\tau e^2\sqrt{m_1m_2m_3}}{\pi^{3/2}\sqrt{2}\hbar^3 m_i\beta^{3/2}} e^{-\chi_n\beta(E_n-\mu)}\delta_{i,j}, \tag{11a}$$

$$[\underline{\boldsymbol{S}}]_{i,j} \sim -\chi_n\frac{k_B}{2e}(5+\chi_n 2\beta(E_n-\mu))\delta_{i,j}. \tag{11b}$$

The corresponding asymptotic expansions in the metallic limit are

$$[\underline{\boldsymbol{\sigma}}]_{i,j} \sim \frac{\tau e^2 2^{3/2}\sqrt{m_1m_2m_3}}{3\pi^2\hbar^3 m_i}(\chi_n(\mu-E_n))^{3/2}\delta_{i,j}, \tag{12a}$$

$$[\underline{\boldsymbol{S}}]_{i,j} \sim \frac{k_B\pi^2}{2e}\frac{1}{\beta(E_n-\mu)}\delta_{i,j}. \tag{12b}$$

Here, E_n represents either a band-edge minimum or maximum, and χ_n is either $+1$ for a conduction-like band, or -1 for a valence-like band.

In order to point to the specific dependence on the effective masses and the carrier density, ρ, we may derive the basic grand-canonical equation of state and invert it to express the chemical potential, μ, in terms of the carrier density, ρ, in both the insulator and metallic limits. For example, for a single conduction-like band,

$$\beta(E_0-\mu) \sim -\ln\left(\frac{\sqrt{2}\hbar^3\pi^{3/2}\beta^{3/2}}{\sqrt{m_xm_ym_z}}\rho\right), \quad \beta(E_0-\mu)\gg 1(\text{insulator}), \tag{13a}$$

$$\beta(E_0-\mu) \sim -\frac{3^{2/3}\hbar^2\pi^{4/3}\beta}{2m_x^{1/3}m_y^{1/3}m_z^{1/3}}\rho^{2/3}, \quad \beta(E_0-\mu)\ll -1(\text{metal}). \tag{13b}$$

One can thus obtain the corresponding asymptotic expressions for the components of $\underline{\boldsymbol{\sigma}}$ and $\underline{\boldsymbol{S}}$ in terms of ρ, namely

$$[\underline{\boldsymbol{\sigma}}]_{i,j} \sim \frac{e^2\tau\rho}{m_i}\delta_{i,j}, \quad \beta(E_0-\mu)\gg 1(\text{insulator}), \tag{14a}$$

$$[\underline{\boldsymbol{S}}]_{i,j} \sim \frac{-k_B}{2e}\left(5-2\ln\left(\frac{\sqrt{2}\hbar^3\pi^{3/2}\beta^{3/2}}{\sqrt{m_xm_ym_z}}\rho\right)\right)\delta_{i,j}, \quad \beta(E_0-\mu)\gg 1(\text{insulator}), \tag{14b}$$

$$[\underline{\boldsymbol{\sigma}}]_{i,j} \sim \frac{e^2\tau\rho}{m_i}\delta_{i,j}, \quad \beta(E_0-\mu)\ll -1(\text{metal}), \tag{14c}$$

$$[\underline{\boldsymbol{S}}]_{i,j} \sim -\frac{k_B\pi^{2/3}m_x^{1/3}m_y^{1/3}m_z^{1/3}}{e3^{2/3}\hbar^2\beta\rho^{2/3}}\delta_{i,j}, \quad \beta(E_0-\mu)\ll -1(\text{metal}) \tag{14d}$$

that, in the isotropic limit, match the more common equations mentioned in the introduction. In particular, in the metallic limit, the relation between the Seebeck coefficient and the electrical conductivity reduces to the expression derived from the Cutler–Mott formula for isotropic bands (Cutler and Mott 1969; Parker, Chen, and Singh 2013; Chen, Parker, and Singh 2013; Filippetti et al. 2012; Snyder and Toberer 2008), namely

$$S = -\frac{k_B}{e\hbar^2}m^*\left(\frac{\pi}{3\rho}\right)^{2/3}. \tag{15}$$

Further, we can compute the powerfactor ($\underline{\boldsymbol{S}}^T\cdot\underline{\boldsymbol{\sigma}}\cdot\underline{\boldsymbol{S}}$) in these limits as well:

$$[\underline{\boldsymbol{S}}^T\cdot\underline{\boldsymbol{\sigma}}\cdot\underline{\boldsymbol{S}}]_{i,j} \sim \frac{\tau\rho k_B^2}{4m_i}\left(5-2\ln\left(\frac{\sqrt{2}\hbar^3\pi^{3/2}\beta^{3/2}}{\sqrt{m_xm_ym_z}}\rho\right)\right)^2\delta_{i,j}, \quad \beta(E_0-\mu)\gg 1(\text{insulator}), \tag{16a}$$

$$[\underline{\boldsymbol{S}}^T\cdot\underline{\boldsymbol{\sigma}}\cdot\underline{\boldsymbol{S}}]_{i,j} \sim \frac{\tau k_B^2\pi^{4/3}}{3^{4/3}\hbar^4\beta^2}\frac{m_x^{2/3}m_y^{2/3}m_z^{2/3}}{\rho^{1/3}m_i}\delta_{i,j}, \quad \beta(E_0-\mu)\ll -1(\text{metal}). \tag{16b}$$

With more than one valley or band, we must use eq. [9] along with eq. [2] to fully capture the behavior of the TE quantities away from the band edges. We may use these expressions (eqs [2] and [9]) to clearly disentangle the contribution to transport due to degenerate bands and anisotropic effective mass tensors.

Preliminary considerations can be done here to elucidate the implications of the anisotropic band structure on the tensorial nature of the transport coefficients. Indeed, it has been extensively argued that valleys with strongly anisotropic effective masses improve TE performance (Bilc et al. 2005; Chung et al. 2003; Bilc et al. 2003).

If only a single electronic band is providing carriers, the conductivity is maximized in the direction of principal axis corresponding to the lighter effective mass. The Seebeck coefficient, on the other hand, is a tensor proportional to the identity that is fully specified by the

determinant of the effective mass tensor. In fact, by comparing eqs [2] and [3] it results that, in a single band case, both $\underline{\mathscr{L}}^{(0)}$ and $\underline{\mathscr{L}}^{(1)}$ are proportional to the same matrix. Since the Seebeck tensor is proportional to $\underline{\mathscr{L}}^{(0)-1} \cdot \underline{\mathscr{L}}^{(1)}$, this results in a Seebeck tensor proportional to the identity matrix. A strongly anisotropic effective mass tensor may provide a large conductivity and a large Seebeck coefficient in different directions. This can be seen directly by considering eq. [14]. We point out that the considerations above hold as sufficient conditions regardless of the specific crystal symmetry. For instance, in a tetragonal crystal the Seebeck tensor will be proportional to the identity matrix if only one valley is contributing carriers. The cancellation, however, does not happen when more non-degenerate bands are active in transport as we will show in the next section.

Effect of Multivalley Band Structure

When several bands are simultaneously contributing to the transport coefficients the complexity is greatly increased. The quantities $\mathscr{L}^{(\alpha)}$ (eq. [2]) are always symmetric tensors because of the Onsager reciprocal relationships implied by microscopic causality and their definition in the Boltzmann transport theory (Mecholsky et al. 2014 and references therein). While this property is straightforwardly transferred to the electrical and thermal conductivity, there are instances when the Seebeck coefficient is (1) not proportional to the identity and (2) not a symmetric tensor.

(1) Let us focus first on eq. [9] considering, for the sake of simplicity, only two bands, A and B, characterized by $\underline{\mathscr{C}}_A$ and $\underline{\mathscr{C}}_B$. In the case where the extrema, E_A and E_B, are degenerate, the function K_α in eq. [8] factorizes out and $\underline{\mathscr{C}}_{A+B} = \underline{\mathscr{C}}_A + \underline{\mathscr{C}}_B$ leading to a Seebeck coefficient proportional to the identity matrix as in the case of single band. Since the Seebeck coefficient is proportional to the identity, all eigenvalues are identical. As soon as the degeneracy between E_A and E_B is lifted, however, the eigenvalues of the Seebeck spread. Regardless of the relative orientation of the principle axes of each band, the $\underline{S}$ tensor has real eigenvalues. If the principle axes happen to be aligned, then both $\underline{\mathscr{C}}_A$ and $\underline{\mathscr{C}}_B$ may be simultaneously diagonalized and the eigenvalues will be real since both $\underline{\mathscr{C}}_A$ and $\underline{\mathscr{C}}_B$ are symmetric. Even though $\underline{\boldsymbol{S}}$ is diagonal, the eigenvalues will in general be different in each direction according to the anisotropy of each band. Figure 1 illustrates the effect of lifting the degeneracy between two conduction bands with arbitrarily chosen effective mass tensors. In the case of degenerate

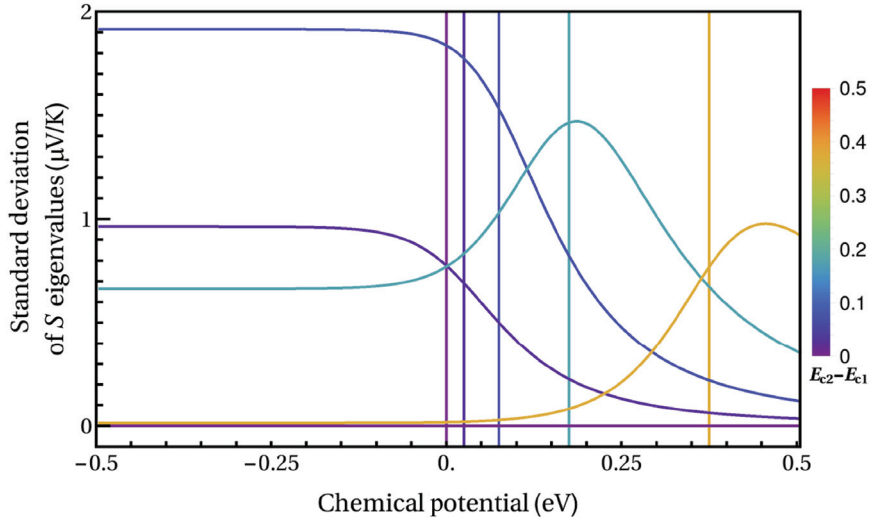

Figure 1: Effect of the lifting of the degeneracy between two ellipsoidal bands with identical effective mass tensors. Standard deviation of the eigenvalues of the thermopower tensor is plotted as a function of the chemical potential, μ, for a model with two highly anisotropic ellipsoidal conduction bands. The two ellipsoidal bands have masses $m_{c1,x} = 0.1, m_{c1,y} = 3, m_{c1,z} = 5$, and $m_{c2,x'} = 0.2, m_{c2,y'} = 7, m_{c2,z'} = 11$, respectively. Both bands have the same set of principal axes. The minimum of the lower conduction band is set at 0 eV and the other conduction-band minimum is set at a variety of energy ranging from 0 to $+0.5$ eV. The color of the curve (identified by the legend) reflects the band spacing (relative energy shift) and the vertical line indicates the beginning of the upper conduction band relative to the lower minimum of the conduction band at 0 eV. Calculations were performed at a fixed temperature $T = 500$ K. The standard deviation of the eigenvalues indicates the deviation from an isotropic case (even for highly anisotropic bands) in which the Seebeck coefficients are proportional to the identity matrix as shown for zero shift.

bands ($E_{c2} - E_{c1} = 0$, purple curve), the eigenvalues of the Seebeck tensor, $\underline{\boldsymbol{S}}$, are identical (with zero standard deviation), however, as a small shift ($E_{c2} - E_{c1} \neq 0$) is imposed between the two conduction-band minima, the standard deviation of the eigenvalues changes unexpectedly. The effect is quantitatively very small with our chosen model parameters which indicates that for some effective masses (even highly anisotropic) there may be a difficulty of detecting the splitting of the eigenvalues experimentally. Similar analysis for the electrical conductivity, $\underline{\boldsymbol{\sigma}}$, reveals the standard deviation of the eigenvalues decreases by increasing the shift between the minima of the conduction bands: this is a consequence of the changes in the number of active carriers. The consequences of crystal symmetry superimpose on the above considerations leading, in a tetragonal material, to a diagonal Seebeck tensor with two identical eigenvalues.

(2) The form of eq. [2a] allows for the possibility of an asymmetric $\underline{\boldsymbol{S}}$ tensor and a larger effect on the standard deviation of its eigenvalues. In Figure 2, we show two such examples with highly anisotropic bands. Each example features a conduction band and a valence band with arbitrarily chosen masses ($m_{v,x} = 0.1, m_{v,y} = 3, m_{v,z} = 5$, and $m_{c,x'} = 0.2$, $m_{c,y'} = 7, m_{c,z'} = 11$) at $T = 500\,\mathrm{K}$ where the valence-band extremum is at −0.5 eV and the conduction-band extremum is at $+0.5$ eV. In the left panels, (a)–(c), the principal axes of both the valence and the conduction bands are chosen to be the coordinate axes. This means that each term in eq. [9] is simultaneously diagonalizable and thus $\underline{\boldsymbol{S}}$ will be diagonal but might have some spread in the eigenvalues. In this case (a special case of (1)), the spread is relatively small. This is evident in panel (c) where all eigenvalues seem equal for any chemical potential μ. Since $\underline{\boldsymbol{\sigma}}$ is proportional to $\underline{\mathscr{L}}^{(0)}$, we see that $\underline{\boldsymbol{\sigma}}$ is diagonal, but not isotropic since the effective masses differ. Compare this with right panels, (d)–(f). In this case, the principal axes are not equivalent and the conduction band is rotated with respect to the valence band. This means that the terms in eq. [9] are not simultaneously diagonalizable. Thus each $\underline{\mathscr{L}}^{(\alpha)}$ is a different linear combination of the same symmetric matrices. This means that each $\underline{\mathscr{L}}^{(\alpha)}$ is symmetric, but their products (see, for instance, $\underline{\boldsymbol{S}}$ from eq. [14] (b)) are only symmetric if the matrices commute. In this case, they do not and the result is that the Seebeck tensor becomes a non-trivial, non-symmetric tensor and the eigenvalues split due mainly to the rotation of the principal axes (see panel (f)). We still see that the conductivity appears unaffected. In a case where the Seebeck tensor is non-symmetric, we are guaranteed by its form (a product of different linear combinations of a set of non-commuting symmetric matrices) to have real eigenvalues but non-orthogonal eigenvectors. These eigenvectors are independent of chemical potential, but depend on the effective masses and orientations of the bands. In contrast to this, since the conductivity is always symmetric and the asymptotic forms are correct inside the valence band and inside the conduction band, the conductivity tensor's principal axes need to transition (as a function of chemical potential) from the principal axes of the valence band to the principal axes of the conduction band. At each chemical potential, the axes need to stay orthogonal to ensure a symmetric conductivity.

To investigate the effect induced by the rotation of the effective mass tensors we discuss a model similar to the one shown in Figure 1 but with the effective mass tensor's principal axes rotated a fixed angle with respect to each other. The rotation greatly magnifies the effect of the relative shift of the conduction-band minima (compare the vertical scales of Figure 3 with Figure 1) on the standard deviation of the eigenvalues of $\underline{\boldsymbol{S}}$. Here we see a jump in the standard deviation from about 2 μV/K to about 50 μV/K. This effect could be used both for optimization purposes and to detect effective mass tensor rotations from transport data. When crystal symmetry is taken into consideration the $\underline{C}$ tensors (eq. [10]) of all the equivalent (degenerate) valleys sum to an effective tensor with the symmetry of the crystal.

Considerations on Realistic Band Structures

We present here two examples of band structures and analyze them from the point of view of the anisotropy of the conductivity and the Seebeck coefficient tensors. We focus on materials that may be interesting for TE application: half-Heusler ZrNiSn and (Sr,Ba)Nb_2O_6 with the tetragonal tungsten bronze structure.

Our electronic structure calculations were performed with the Quantum Espresso (QE) package (Giannozzi et al. 2009) using ultrasoft PBE pseudopotentials, a

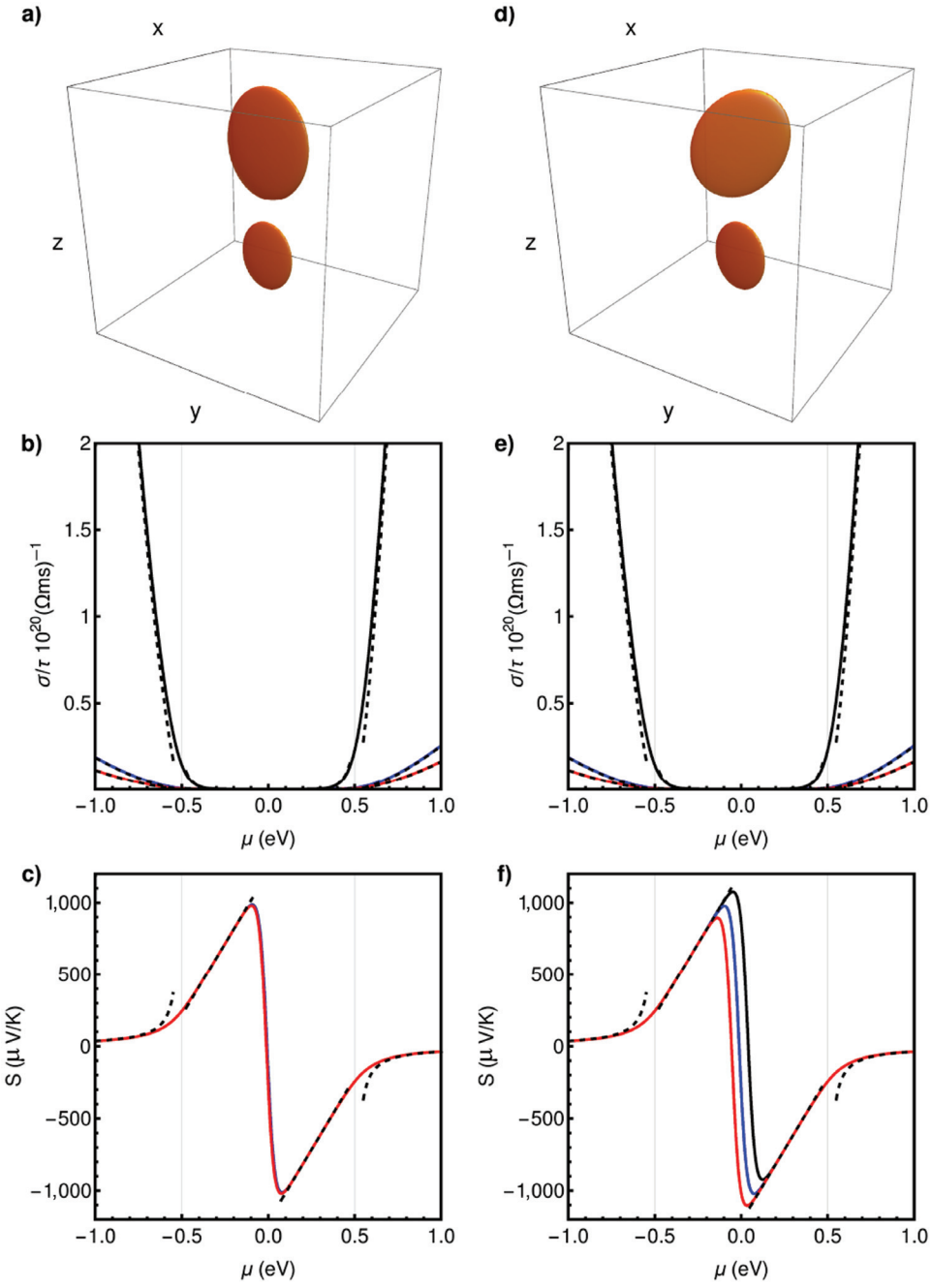

Figure 2: Conductivity and thermopower tensor eigenvalues for a model with two highly anisotropic ellipsoidal bands. The two ellipsoidal bands have masses $m_{v,x} = 0.1, m_{v,y} = 3, m_{v,z} = 5$, and $m_{c,x'} = 0.2, m_{c,y'} = 7, m_{c,z'} = 11$, respectively. In plots (a)–(c) the principal axes of the conduction band and valence band are the coordinate axes. In plots (d)–(f), the principal axes are rotated with respect to those of the valence band through Euler angles $\Phi = \pi/7$, $\Theta = \pi/6$ and $\Psi = 0$. Two constant energy surfaces for the two bands are shown in panels (a) and (d). The valence-band maximum is set at –0.5 eV and the conduction-band minimum is set at $+0.5$ eV. Panels (b)–(c) and (e)–(f) show three curves each, representing the three eigenvalues of the conductivity tensor, normalized by the relaxation time, τ, and of the thermopower tensor, as functions of the chemical potential, μ for each case. The absolute temperature is set at $T = 500$ K. One-band asymptotic expansions from eq. [14] are represented by black dashed curves.

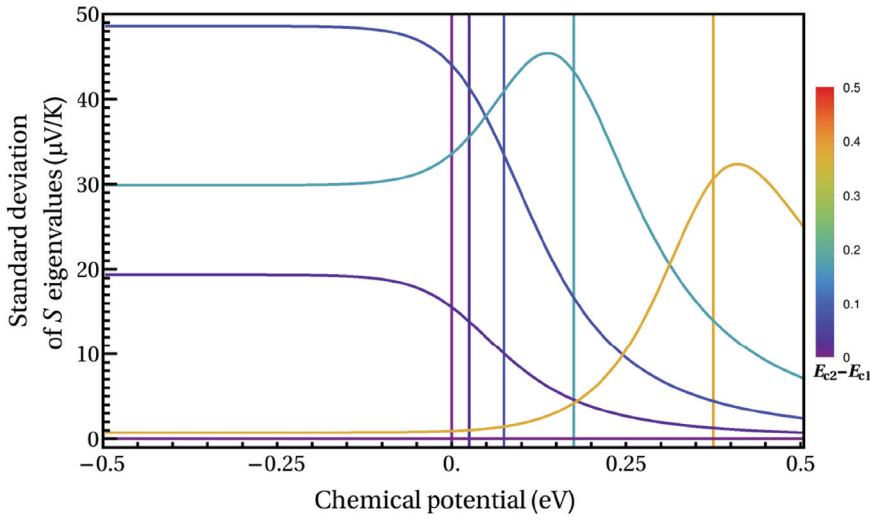

Figure 3: Effect of the lifting of the degeneracy between two ellipsoidal bands with effective mass tensors that are rotated with respect to each other. The standard deviation of the eigenvalues indicates the deviation from an isotropic case in which the Seebeck coefficients are proportional to the identity matrix as shown for zero shift. The two ellipsoidal bands have masses $m_{c1,x} = 0.1, m_{c1,y} = 3, m_{c1,z} = 5$, and $m_{c2,x'} = 0.2, m_{c2,y'} = 7, m_{c2,z'} = 11$, respectively. The principal axes are rotated with respect to those of the lower conduction band through Euler angles $\Phi = \pi/7$, $\Theta = \pi/6$ and $\Psi = 0$. The minimum of the lower conduction band is set at 0 eV and the other conduction-band minimum is set at a variety of energies ranging from 0 to $+0.5$ eV. The color of the curve (identified by the legend) determines the band spacing and the vertical line indicates the beginning of the upper conduction band. The absolute temperature is set at $T = 500$ K.

well-converged basis set and appropriate BZ sampling. The transport coefficients were computed within the constant scattering-time approximation as implemented in BolzTrap (Madsen and Singh 2006).

Half-Heusler alloys have a chemical formula of XYZ, where X and Y are transition or rare-earth metals and Z is an sp element crystallized in a cubic structure (space group no. 216). These alloys exhibit a lower TE power-factor as compared with other materials but they are very stable with respect to alloying and doping and greatly optimizable. Half-Heusler alloys such as XNiSn (X = Ti, Zr, Hf) are semiconductors with narrow band gaps in the range 0.1–0.2 eV and heavy carrier mass (Uher et al. 1999). They have relatively high lattice thermal conductivity that can be suppressed by the substitution with isoelectronic elements at the X-site due to phonon scattering (Zou et al. 2013; Wee et al. 2012). While doping at the Zr site reduces the lattice thermal conductivity, doping on the Sn site tunes carrier concentration (Yu et al. 2009; Kim, Kimura, and Mishima 2007; Kawaharada et al. 2004). The band structure of ZrNiSn is presented in Figure 4. The valence band is characterized by two degenerate Γ valley (note that degeneracy may lead to warping effects not discussed in this paper, see Mecholsky et al. (2014). Away from Γ the band decreases in energy and flattens leading to a larger average effective mass. This leads to a relatively larger thermopower in

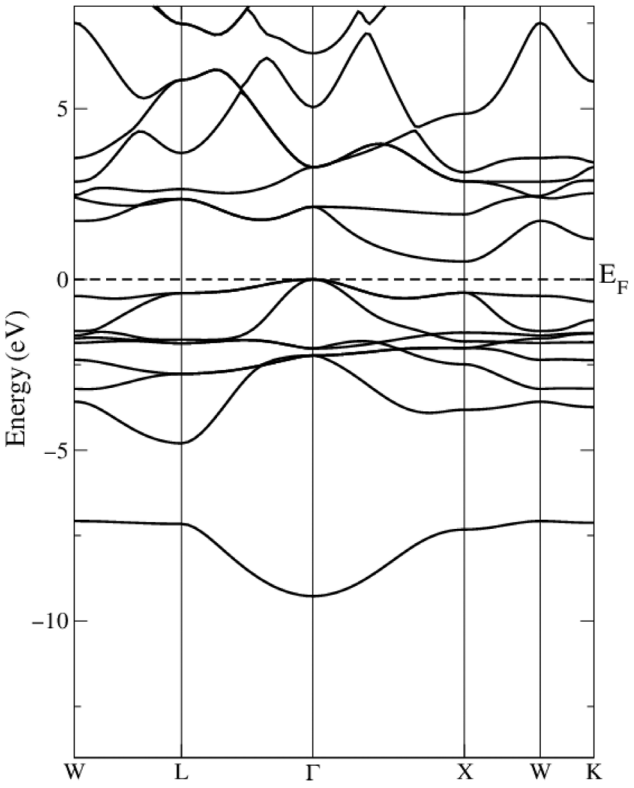

Figure 4: Band structure of half-Heusler ZrNiSn computed with the Quantum Espresso package. The limited band dispersion at the top of the valence band leads to large thermopower. The cubic symmetry forces, as expected, the transport tensor to be proportional to the identity.

case of p-type doping. The conduction band is characterized by a single band. The electrical conductivity and the thermopower are proportional to the identity matrix even at high temperature (700 K) and for substantially different doping indicating, as expected, that cubic crystal symmetry determines the anisotropy regardless of band degeneracies (Figure 5).

$Sr_{0.6}Ba_{0.4}Nb_2O_6$ (SBN6) is an oxide recently studied for its TE potentials (Lee et al. 2011). The interesting material belongs structurally to the tetragonal tungsten–bronze family and is strongly anisotropic because the *c*-axis is 3–4 times smaller than the lattice parameter *a* (space group no. 100). The band structure near the band gap is shown in Figure 6 and involves a mostly *p*-character manifold at the top of the valence band and a conduction band with relative large *d*-states contribution from the Nb. The large structural anisotropy is reflected in the Γ-Z direction. The conductivity is much larger along the *c*-axis due to the large Γ-Z dispersion for both electrons and holes. Even though the band structure plot is an imperfect representation of anisotropy, the anisotropy is evident and confirmed from the diagonal elements of the conductivity tensor. For p-type doping there are several bands active in transport at 700 K (~60 meV) and the thermopower tensor exhibits different values for the diagonal terms (that are enormous because of the large effective masses). In the case of n-type doping the effect is less pronounced.

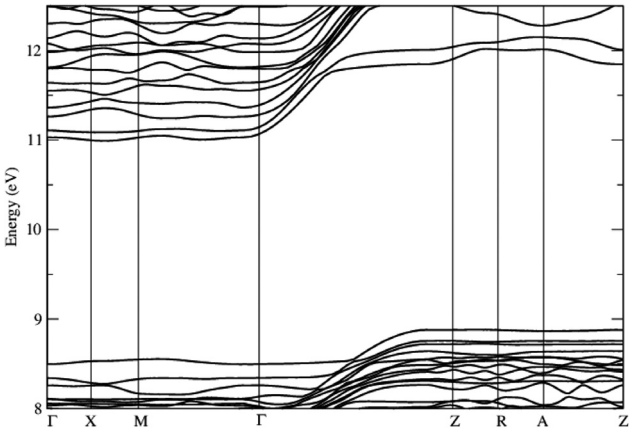

Figure 6: Band structure of $Sr_{0.6}Ba_{0.4}Nb_2O_6$ below and above the forbidden energy gap. The calculations were performed with the Quantum Espresso package. The larger dispersion in the *Γ*-Z direction leads to a larger conductivity along the *c*-axis. The large effective masses for both the conduction and the valence bands justifies the enormous thermopower, Figure 7.

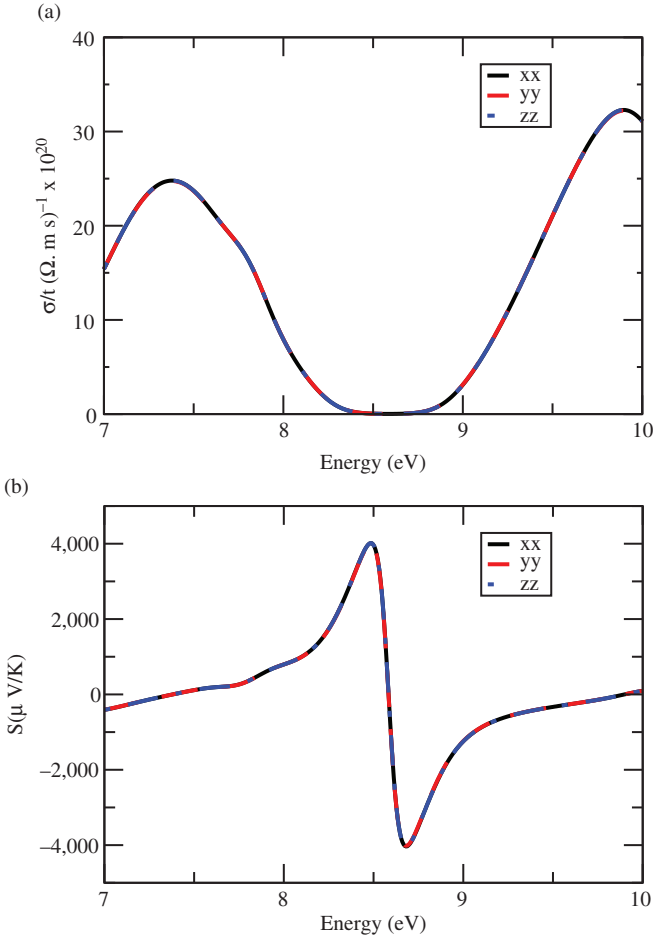

Figure 5: Diagonal terms of the conductivity and Seebeck tensors at $T = 700$ K of half-Heusler ZrNiSn vs the chemical potential (in eV). The diagonal values of the thermopower tensors are proportional to the identity due to the cubic symmetry.

Conclusions

The general tensorial transport theory developed by Mecholsky et al. (2014) is applied to understand the band structure conditions leading to thermopower tensors that are not proportional to the identity matrix. Although the electrical conductivity is always a symmetric tensor and inherits the anisotropy from the symmetry of the band structure, the Seebeck coefficient is anisotropic (and in fact non-symmetric) only when several bands are contributing to the transport and their effective mass ellipsoids cannot be diagonalized simultaneously. The observation of the spread of the eigenvalues of the Seebeck tensor provides a method to derive information on the relative orientation of the principal axis of the ellipsoids representing the effective masses. The results are in agreement with band structure calculations.

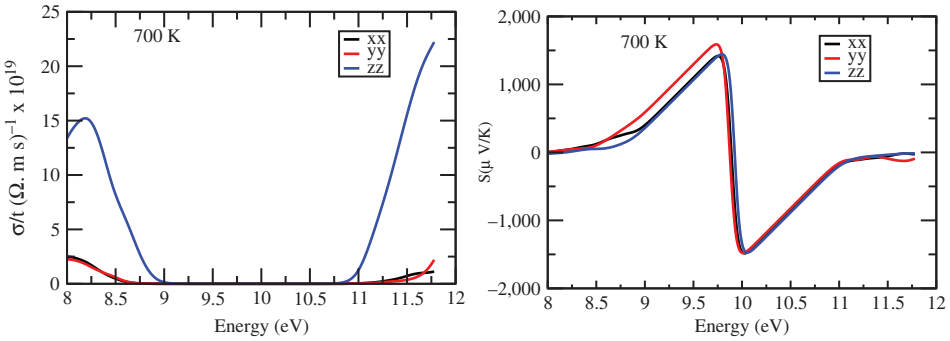

Figure 7: Diagonal terms of the conductivity and Seebeck tensors at $T = 700$ K for $Sr_{0.6}Ba_{0.4}Nb_2O_6$ vs the chemical potential (in eV). The larger conductivity along the *c*-axis of the tetragonal cell is justified by the larger Γ-Z dispersion as compared with in-plane bands. The spread of the diagonal values of the thermopower tensors are supporting the predictions of the analytical models discussed in the text. Minor deviation from ideal crystal symmetry are due to numerical errors.

Acknowledgments: MF acknowledges collaboration with the AFLOW consortium under the sponsorship of DOD-ONR (N000141310635). We are grateful to M. Buongiorno Nardelli and D. Singh for useful suggestions.

Funding: This work was performed with the sponsorship of the Vitreous State Laboratory of the Catholic University of America.

References

Ashcroft, N. W., and N. D. Mermin. 1976. *Solid State Physics*. 1st ed. Philadelphia, PA: W. B. Saunders Company.

Bilc, D. I., P. Larson, S. D. Mahanti, and M. G. Kanatzidis. 2003. *Effect of K/Bi ordering on the electronic structure of $K_2Bi_8Se_{13}$*. In: *Mat. Res. Soc. Symp. Proc. (MRS Proceedings)*, Vol. 793, S6–5. Cambridge Univ. Press. S6.5.1–S6.5.6.

Bilc, D. I., S. D. Mahanti, Th. Kyratsi, D. Y. Chung, M. G. Kanatzidis, and P. Larson. 2005. "Electronic Structure of $K_2Bi_8Se_{13}$." *Physical Review B* 71 (8): 085116.

Chen, X., D. Parker, and D. J. Singh. 2013. "Importance of Non-parabolic Band Effects in the Thermoelectric Properties of Semiconductors." *Scientific Reports* 3: 3168.

Chung, D.-Y., S. D. Mahanti, W. Chen, C. Uher, and M. G. Kanatzidis. 2003. *Anisotropy in Thermoelectric Properties of $CsBi_4Te_6$*. In: *MRS Proceedings*, Vol. 793, S6–1. Cambridge Univ. Press.

Cutler, M., and N. F. Mott. 1969. "Observation of Anderson Localization in an Electron Gas." *Physical Review* 181 (3): 1336.

Filippetti, A., P. Delugas, M. J. Verstraete, I. Pallecchi, A. Gadaleta, D. Marré, D. F. Li, S. Gariglio, and V. Fiorentini. 2012. "Thermopower in Oxide Heterostructures: The Importance of Being Multiple-Band Conductors." *Physical Review B* 86 (19): 195301.

Giannozzi, P., S. Baroni, N. Bonini, M. Calandra, R. Car, C. Cavazzoni, D. Ceresoli, G. L. Chiarotti, M. Cococcioni, I. Dabo, et al. 2009. "Quantum Espresso: A Modular and Open-Source Software Project for Quantum Simulations of Materials." *Journal of Physics: Condensed Matter* 21 (39): 395502 (19pp).

Grosso, G., and G. Pastori Parravicini. 2000. *Solid State Physics*. 1st ed. San Diego, CA: Academic Press.

Kanatzidis, M. G. 2009. "Nanostructured Thermoelectrics: The New Paradigm?" *Chemistry of Materials* 22 (3): 648–59.

Kawaharada, Y., H. Uneda, H. Muta, K. Kurosaki, and S. Yamanaka. 2004. "High Temperature Thermoelectric Properties of Nizrsn Half-Heusler Compounds." *Journal of Alloys and Compounds* 364 (1): 59–63.

Kim, S.-W., Y. Kimura, and Y. Mishima. 2007. "High Temperature Thermoelectric Properties of TiNiSn-Based Half-Heusler Compounds." *Intermetallics* 15 (3): 349–56.

Lee, S., S. Dursun, C. Duran, and C. A. Randall. 2011. "Thermoelectric Power Factor Enhancement of Textured Ferroelectric $Sr_xBa_{1-x}Nb_2O_{6-\Delta}$ Ceramics." *Journal of Materials Research* 26 (1): 26–30.

Madsen, G. K. H. and D. J. Singh. 2006. "Boltztrap. A Code for Calculating Band-Structure Dependent Quantities." *Computer Physics Communication* 175 (1): 67–71.

Mecholsky, N. A., L. Resca, I. L. Pegg, and M. Fornari. 2014. "Theory of Band Warping and Its Effects on Thermoelectronic Transport Properties." *Physical Review B* 89: 155131.

Nolas, G. S., J. Poon, and M. Kanatzidis. 2006. "Recent Developments in Bulk Thermoelectric Materials." *MRS Bulletin* 31 (3): 199–205.

Nolas, G. S., J. Sharp, and J. Goldsmid. 2001. *Thermoelectrics: Basic Principles and New Materials Developments*. *Springer Series in Materials Science*, Vol. 45. Berlin Heidelberg: Springer-Verlag.

Parker, D., X. Chen, and D. J. Singh. 2013. "High Three-Dimensional Thermoelectric Performance From Low-Dimensional Bands." *Physical Review Letters* 110: 146601.

Singleton, J. 2001. *Band Theory and Electronic Properties of Solids*. Oxford: Oxford University Press.

Snyder, G. J., and E. S. Toberer. 2008. "Complex Thermoelectric Materials." *Nature Materials* 7 (2): 105–14.

Uher, C., J. Yang, S. Hu, D. T. Morelli, and G. P. Meisner. 1999. "Transport Properties of Pure and Doped MNiSN (M = Zr, Hf)." *Physical Review B* 59 (13): 8615.

Wee, D., B. Kozinsky, B. Pavan, and M. Fornari. 2012. "Quasiharmonic Vibrational Properties of Tinisn from Ab Initio Phonons." *Journal of Electronic Materials* 41 (6): 977–83.

Yu, C., T.-J. Zhu, R.-Z. Shi, Y. Zhang, X.-B. Zhao, and J. He. 2009. "High-Performance Half-Heusler Thermoelectric Materials $Hf_{1-x}Zr_xNiSn_{1-y}Sb_y$ Prepared by Levitation Melting and Spark Plasma Sintering." *Acta Materialia* 57 (9): 2757–64.

Zou, D. F., S. H. Xie, Y. Y. Liu, J. G. Lin, and J. Y. Li. 2013. "Electronic Structure and Thermoelectric Properties of Half-Heusler $Zr_{0.5}hf_{0.5}NiSn$ by First-Principles Calculations." *Journal of Applied Physics* 113 (19): 193705.